

Hanbury Brown and Twiss correlations across the Bose-Einstein condensation threshold

A. Perrin,^{1,2} R. Bücker,¹ S. Manz,¹ T. Betz,¹ C. Koller,¹ T. Plisson,^{1,3} T. Schumm,^{1,2} and J. Schmiedmayer¹

¹Vienna Center for Quantum Science and Technology, Atominstitut, TU Wien, 1020 Vienna, Austria

²Wolfgang Pauli Institute, 1090 Vienna, Austria

³Laboratoire Charles Fabry de l'Institut d'Optique, Univ Paris Sud, CNRS, Campus Polytechnique RD128, 91127 Palaiseau, France

(Dated: May 16, 2022)

Hanbury Brown and Twiss correlations, i.e. correlations in far-field intensity fluctuations, yield fundamental information on the nature of light sources, as highlighted after the discovery of photon bunching. Drawing on the analogy between photons and atoms, comparable observations have been made studying expanding Bose gases. We have used two-point density correlations to study how matter-wave coherence is established when crossing the Bose-Einstein condensation threshold. Our experiments reveal a persistent multimode character of the source, also significantly below the condensation threshold temperature. Complex quantum correlations are observed for a variety of source geometries, from quasi-isotropic to highly elongated. Ideal Bose gas theory reproduces most of the qualitative features of our measurements, however a quantitative analysis highlights the need for a more comprehensive theoretical description including particle interactions.

Hanbury Brown and Twiss (HBT) correlations of thermal light can be related to a quantum interference effect reflecting the multimode nature of the source [1–3]. For a monomode laser they are essentially absent, yielding only poissonian shot noise [8]. In analogy to chaotic light sources, atom bunching in expanding thermal Bose gases has been observed [4–7]. Poissonian noise statistics of an expanding Bose-Einstein condensate (BEC) [6] or an atom-laser [9] have been reported, comparable to a monomode optical laser. Yet, studies of coherence of Bose gases near the phase transition have been limited to the analysis of first order correlations [10, 11]. The measurements reported in this letter focus on two-point density correlations of expanding Bose gases near the BEC threshold and stress the finite coherence of these systems while covering different regimes of atomic quantum gases, associated with ‘1D’ and ‘3D’ physics. A simple model based on ideal Bose gas theory [12] reflects the basic properties of our observations in the case of essentially isotropic sources. For very elongated gases the model fails quickly below the BEC threshold, confirming the major role of interactions in this regime [13–17]. Our findings illustrate that realizing a true matter-wave analogue to the single mode laser, an important step for interferometry and metrology applications [18], still represents an experimental challenge.

Density fluctuations are typically characterized by the second order correlation function $g_2(\mathbf{r}, \mathbf{r}')$, which measures the probability of joint detection of two particles at positions \mathbf{r} and \mathbf{r}' . In absence of two-particle correlations, $g_2(\mathbf{r}, \mathbf{r}') = 1$. Otherwise g_2 reflects the spatial scales of the density fluctuations. For an ideal Bose gas crossing the BEC threshold, g_2 is expected to flatten out to unity, while the coherence lengths of the system diverge [12, 19]. This behaviour is in close analogy to a laser crossing the threshold. Taking into account particle

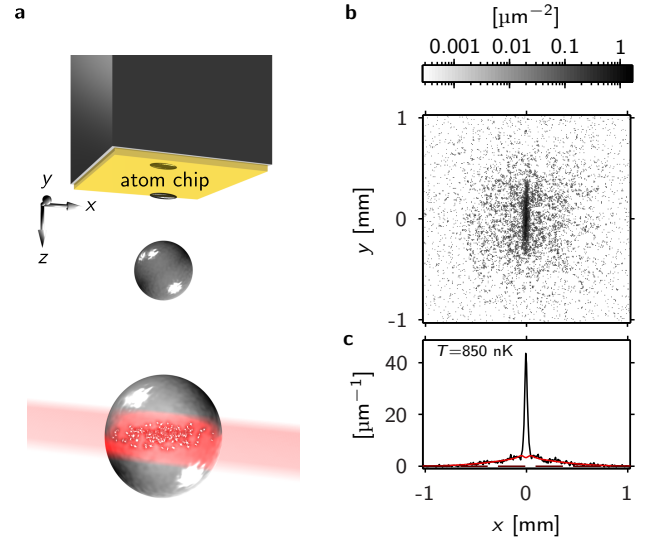


FIG. 1. **a**, Schematic of the experimental geometry. **b**, Example of the density distribution (lateral cut, log scale) of a Bose gas slightly below the Bose-Einstein condensation threshold after 46 ms expansion time. **c**, Profile of **b**, integrated along y . The red line indicates a fit to the density distribution of the thermal fraction, yielding the temperature T .

interactions renders theoretical descriptions very difficult because of the large number of modes which have to be taken into account for finite temperature systems. Furthermore, hydrodynamic effects during expansion complicate the problem. In the following we will restrict the analysis to ideal Bose gas theory and only qualitatively comment on effects of interactions.

We prepare ^{87}Rb gases in the $|F, m_F\rangle = |1, -1\rangle$ state in an atom chip magnetic trap at temperatures close to the BEC threshold [20]. The chip design allows us to control the parameters of the magnetic trap and hence the shape

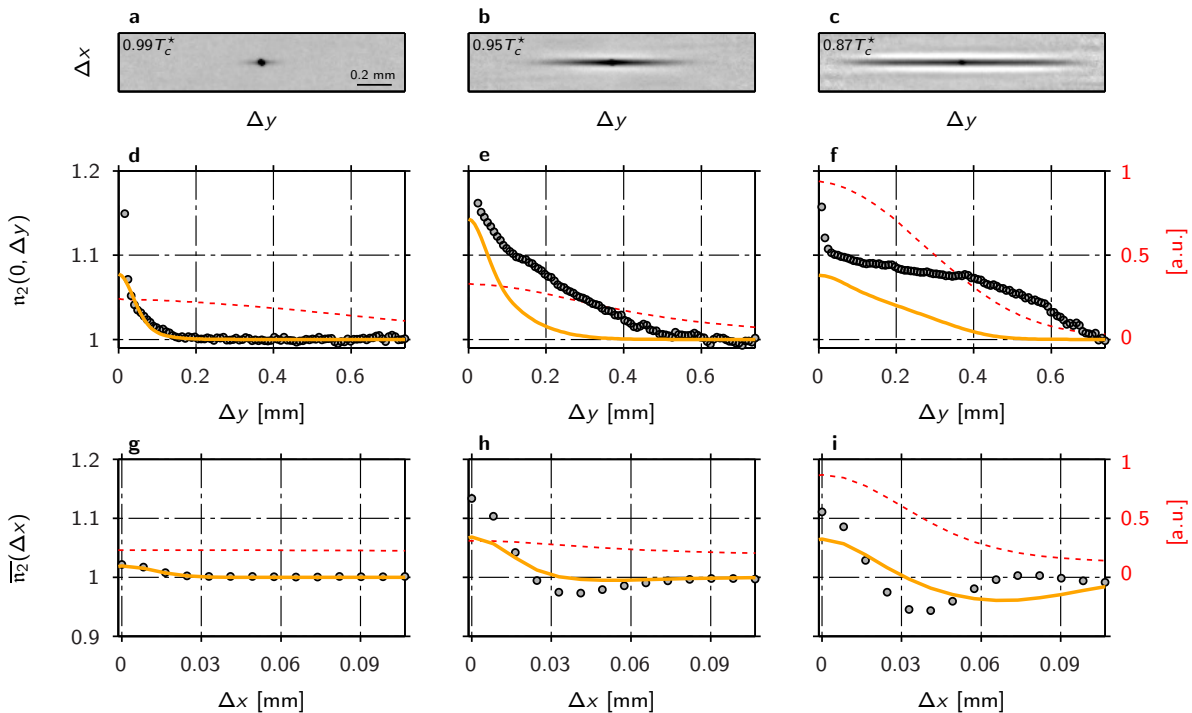


FIG. 2. **a,b,c**, Density correlation functions of expanding Bose gases n_2 (lateral cut in $(\Delta x, \Delta y)$ plane) at $0.99 T_c^*$, $0.95 T_c^*$, and $0.85 T_c^*$, the aspect ratio λ of the atomic source is 13.5. **d,e,f**, (circles) Radial cuts of **a,b** and **c**. (dashed line) Radial cuts of the corresponding autocorrelation of the mean density profile. (solid line) Radial cuts of ideal Bose gas theory's predictions for the second order correlation function $g_2(0, \Delta y)$. **g,h,f**, (circles) Radially averaged axial cuts of **a,b** and **c** over $160 \mu\text{m}$ where the shot noise peak \mathfrak{s} is excluded. The width of the exclusion region is $32 \mu\text{m}$. (dashed line) Radially averaged axial cuts of the corresponding autocorrelation of the mean density profile. (solid line) Radially averaged axial cuts of ideal Bose gas theory's predictions for the second order correlation function $\overline{g_2}(\Delta x)$.

of the matter-wave source over a large range of aspect ratios $\lambda = \omega_{y,z}/\omega_x$ from 4 to 120, where ω_x and $\omega_{y,z}$ are the axial and radial trap frequencies respectively [21]. To obtain the second order correlation function of a Bose gas after its release from the trap, we use a novel fluorescence imaging [22] which allows to record a thin slice of the atomic density in the horizontal x - y plane at the central part of the gas after 46 ms expansion (see Fig. 1a-b). The thickness of the slice is set to $225 \mu\text{m}$ by adjusting the duration of the excitation pulse to $500 \mu\text{s}$.

We obtain the temperature of the system T and deduce the number of atoms in the thermal fraction of the gas N_{th} by fitting the thermal tails of the axial (x axis) density profiles using an analytical formula based on ideal Bose gas theory (see Fig. 1c). By comparing the fit result to the total observed signal, this also yields the number of condensed atoms (if present) within the density slice. A simple model for the expansion of the degenerate fraction of the gas yields N_{bec} , the total number of condensed atoms. Finally, for each set of temperature T and total atom number $N = N_{\text{th}} + N_{\text{bec}}$, we estimate the critical temperature of the system T_c^* through the relation $T_c^* = \alpha^{1/3} T_c$, where $T_c(T, N)$ corresponds to ideal Bose gas theory predictions for the critical temperature. The experimentally obtained factor α depends on the source

aspect ratio λ , but not on N (see Supplementary Material).

Averaging over typically one hundred experimental repetitions with identical parameters, we calculate the mean autocorrelation of the density profiles and normalize it by the autocorrelation of the mean density profile. We obtain the normalized density correlation function n_2 , which can be decomposed into the sum of two terms, \mathfrak{s} and g_2 . The term g_2 contains the desired information about two-particle correlations whereas \mathfrak{s} is a contribution due to atomic shot noise (see Supplementary Material).

Typical results of density correlation functions of expanding Bose gases from a moderately anisotropic source ($\lambda = 13.5$) are shown in Fig. 2. The atomic shot noise \mathfrak{s} appears as a dark oval spot at the center of the function. Its eigen-axes are rotated by 45° with respect to the axes of the atomic source x, y , corresponding to the direction of the imaging laser beams. The structure corresponding to g_2 is visible behind this central spot. Its anisotropy reflects the aspect ratio of the source gas.

Radially (y axis), the RMS width of the g_2 peak rapidly grows when crossing the critical temperature T_c^* until it saturates due the finite radial size of the system (see Fig. 2d-f). This can be seen as an experimental observa-

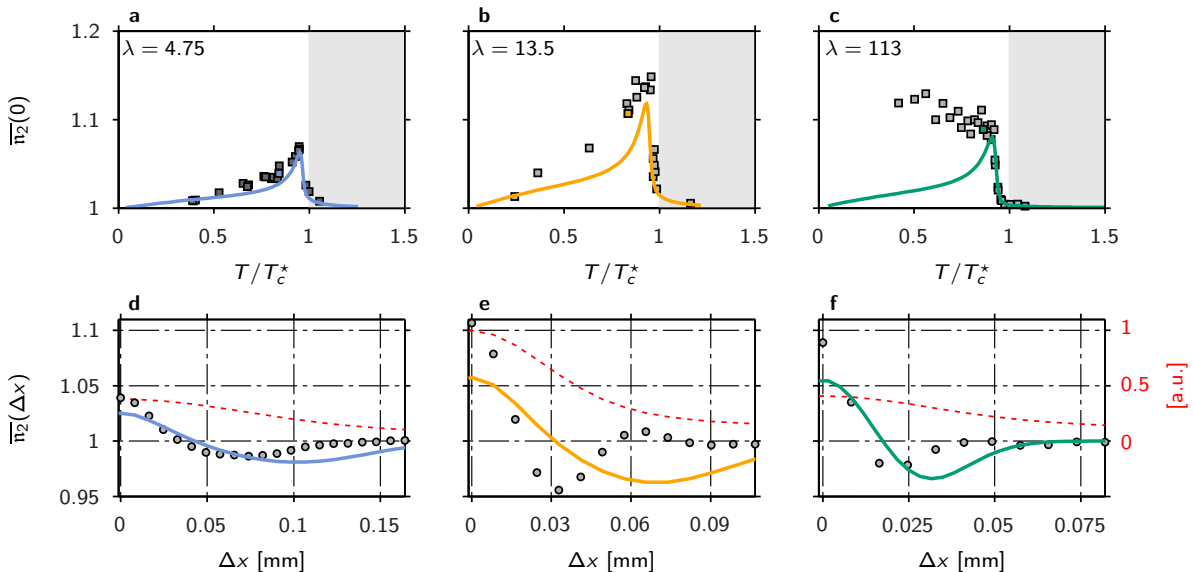


FIG. 3. **a,b,c**, Peak height of the second order correlation function of expanding Bose gases for various ratios T/T_c^* and three different trap aspect ratios $\lambda = 4.75$ (light blue), 13.5 (orange) and 113 (green). It is defined as $\overline{n_2}(0)$ (see caption Fig. 2). The solid lines indicate the predictions obtained from ideal Bose gas theory. The light gray area display the range where the source is fully thermal. Note that the total atom number N is not held constant between the data points, however this is taken into account in the value of T_c^* . **d,e,f**, (circles) Radially averaged axial cuts of the density correlation function $\overline{n_2}$ (see caption Fig. 2) which parameters correspond to the colored square displayed respectively in **a,b** and **c**. (dashed line) Radially averaged axial cuts of the corresponding autocorrelation of the mean density profile. (solid line) Radially averaged axial cuts of ideal Bose gas theory's predictions for the second order correlation function $\overline{g_2}(\Delta x)$.

tion of the establishment of radial coherence [11], where the shape of \mathbf{n}_2 changes from a decreasing exponential (Fig. 2**d-e**) to a profile set by the spatial shape of the condensed cloud after expansion (Fig. 2**f**). The RMS width of the \mathbf{g}_2 peak is related to the radial coherence length in the trapped system through the hydrodynamic expansion of the gas, which imposes a scaling factor on the radial size of the cloud (about 625 here, see Supplementary Material).

Axially (x axis), depending on the trap anisotropy, thermal excitations of the system will typically be spread over more modes than radially. Below but close to the BEC threshold, few of the lowest lying axial modes will get macroscopically occupied and the shape of the second order correlation function \mathbf{g}_2 can then be interpreted as a result of the beating of the contributing modes after expansion. A consequence is the appearance of a dip below unity at finite distance Δx along the \mathbf{g}_2 axial profiles (see Fig. 2**h-i**). A similar behaviour has been reported in recent experiments and theoretical work on 1D Bose gases [17, 23].

Using the thermodynamical properties obtained from the data used to compute \mathbf{n}_2 , we can simulate the second order correlation function \mathbf{g}_2 within ideal Bose gas theory and take into account the imaging resolution [12]. Without any free parameters, we observe an almost perfect agreement with the experimental observations close to or above the BEC threshold, where inter-particles inter-

actions are weak. Below the critical temperature, ideal Bose gas theory still reproduces the qualitative features of the experimental observation: (1) the establishment of coherence along the transverse direction; (2) the appearance of a dip below unity at finite distances along the axial \mathbf{g}_2 (see Fig. 2**d-i**). We attribute the quantitative differences between the observations and the ideal Bose gas theory to interactions (see also Fig. 3**d-f**).

In order to explore the physics of density fluctuations in more details we have repeated the same measurements varying the source geometry and for different ratios of T/T_c^* . For moderate trap aspect ratios ($\lambda = 4.75, 13.5$), the amplitude of the density fluctuations observed in the far field is reduced slowly with decreasing temperature as shown in Fig. 3**a-b**. This behaviour indicates the gradual reduction of the population of the non-condensed fraction of the system below the BEC threshold. It is fairly well reproduced within ideal Bose gas theory. For strongly anisotropic sources ($\lambda = 113$) we observe no reduction of the far-field density fluctuations of the gas with decreasing temperature, in strong contrast to ideal Bose gas theory (see Fig. 3**c**). This behaviour is expected for 1D systems where low lying axial excitations of the system remain macroscopically occupied well below the degeneracy temperature [17, 23].

In conclusion, we are convinced that measurements of density correlations of expanding Bose gases realize a very sensitive probe for excitations and multi-mode prop-

erties of interacting many-body quantum systems. Once a complete theoretical description of interacting Bose gas density fluctuations in expansion is at hand, this method will allow a detailed characterization of the mode occupation of the source. For equilibrium systems, this can be used for precision thermometry well below the critical temperature (see e.g. [17]). For temperatures well below the chemical potential, it would allow to probe quantum fluctuations, e.g. quantum depletion, of 3D or 1D Bose gases. Our studies can directly be extended to non-equilibrium situations in various interaction regimes, where fundamental questions on thermalization and integrability arise [24–26].

We acknowledge support from the Wittgenstein prize, FWF projects F40, P21080-N16 and P22590-N16, the EU projects AQUITE and Marie Curie (FP7 GA no. 236702), the FWF doctoral program CoQuS (W 1210), the EUROQUASAR QuDeGPM Project and the FunMat research alliance. We wish to thank A. Aspect, D. Boiron, A. Gottlieb, I. Mazets, J. Vianna Gomes and C. I. Westbrook for stimulating discussions.

-
- [1] R. Hanbury Brown and R. Q. Twiss, *Nature* **177**, 27 (1956).
- [2] R. Glauber, *Phys. Rev.* **130**, 2529 (1963).
- [3] U. Fano, *Am. J. Phys.* **29**, 539 (1961).
- [4] M. Yasuda and F. Shimizu, *Phys. Rev. Lett.* **77**, 3090 (1996).
- [5] S. Fölling, F. Gerbier, A. Widera, O. Mandel, T. Gericke, and I. Bloch, *Nature* **434**, 481 (2005).
- [6] M. Schellekens, R. Hoppeler, A. Perrin, J. Viana Gomes, D. Boiron, A. Aspect, and C. I. Westbrook, *Science* **310**, 648 (2005).
- [7] T. Jelten, J. M. McNamara, W. Hogervorst, W. Vassen, V. Krachmalnicoff, M. Schellekens, A. Perrin, H. Chang, D. Boiron, A. Aspect, and C. I. Westbrook, *Nature* **445**, 402 (2007).
- [8] F. Arecchi, *Phys. Rev. Lett.* **15**, 912 (1965).
- [9] A. Öttl, S. Ritter, M. Köhl, and T. Esslinger, *Phys. Rev. Lett.* **95**, 4 (2005).
- [10] I. Bloch, T. Hänsch, and T. Esslinger, *Nature* **403**, 166 (2000).
- [11] T. Donner, S. Ritter, T. Bourdel, A. Öttl, M. Köhl, and T. Esslinger, *Science* **315**, 1556 (2007).
- [12] J. Viana Gomes, A. Perrin, M. Schellekens, D. Boiron, C. I. Westbrook, and M. Belsley, *Phys. Rev. A* **74**, 53607 (2006).
- [13] D. Petrov, G. V. Shlyapnikov, and J. Walraven, *Phys. Rev. Lett.* **87**, 50404 (2001).
- [14] S. Dettmer, D. Hellweg, P. Ryytty, J. J. Arlt, W. Ertmer, K. Sengstock, D. Petrov, G. V. Shlyapnikov, H. Kreutzmann, L. Santos, and M. Lewenstein, *Phys. Rev. Lett.* **87**, 160406 (2001).
- [15] S. Richard, F. Gerbier, J. H. Thywissen, M. Hugbart, P. Bouyer, and A. Aspect, *Phys. Rev. Lett.* **91**, 10405 (2003).
- [16] J.-B. Trebbia, J. Estève, C. I. Westbrook, and I. Bouchoule, *Phys. Rev. Lett.* **97**, 250403 (2006).
- [17] S. Manz, R. Bücker, T. Betz, C. Koller, S. Hofferberth, I. E. Mazets, A. Imambekov, E. Demler, A. Perrin, J. Schmiedmayer, and T. Schumm, *Phys. Rev. A* **81**, 031610 (2010).
- [18] A. Cronin, J. Schmiedmayer, and D. E. Pritchard, *Rev. Mod. Phys.* **81**, 1051 (2009).
- [19] M. Naraschewski and R. Glauber, *Phys. Rev. A* **59**, 4595 (1999).
- [20] R. Folman, P. Krüger, J. Schmiedmayer, J. Denschlag, and C. Henkel, *Adv. At. Mol. Phys.* **48**, 263 (2002).
- [21] M. Trinker, S. Groth, S. Haslinger, S. Manz, T. Betz, S. Schneider, I. Bar-Joseph, T. Schumm, and J. Schmiedmayer, *Appl. Phys. Lett.* **92**, 254102 (2008).
- [22] R. Bücker, A. Perrin, S. Manz, T. Betz, C. Koller, T. Plisson, J. Rottmann, T. Schumm, and J. Schmiedmayer, *New J. Phys.* **11**, 103039 (2009).
- [23] A. Imambekov, I. E. Mazets, D. Petrov, V. Gritsev, S. Manz, S. Hofferberth, T. Schumm, E. Demler, and J. Schmiedmayer, *Phys. Rev. A* **80**, 33604 (2009).
- [24] I. E. Mazets, T. Schumm, and J. Schmiedmayer, *Phys. Rev. Lett.* **100**, 210403 (2008).
- [25] M. Rigol, V. Dunjko, and M. Olshanii, *Nature* **452**, 854 (2008).
- [26] I. E. Mazets and J. Schmiedmayer, *New J. Phys.* **12**, 055023 (2010).
- [27] M. Davis and P. B. Blakie, *Phys. Rev. Lett.* **96**, 60404 (2006).
- [28] K. Kheruntsyan, D. Gangardt, P. D. Drummond, and G. V. Shlyapnikov, *Phys. Rev. Lett.* **91**, 40403 (2003).
- [29] Y. Castin and R. Dum, *Phys. Rev. Lett.* **77**, 5315 (1996).
- [30] Y. Kagan, E. Surkov, and G. V. Shlyapnikov, *Phys. Rev. A* **54**, R1753 (1996).

SUPPLEMENTARY MATERIAL

Experimental Setup

We prepare ultracold gases of a few 10^4 ^{87}Rb atoms in the $|F, m_F\rangle = |1, -1\rangle$ state confined in a highly anisotropic Ioffe-Pritchard type magnetic trap on a multilayer atom chip [21]. The trapping frequencies are $\omega_x = 2\pi \times 20$ Hz axially and $\omega_{y,z} = 2\pi \times 2260$ Hz radially ($\lambda = 113$). Using an additional chip wire orthogonal to the main trapping wire allows to load the atoms into a dimple trap with a larger axial frequency of $\omega_x = 2\pi \times 160$ Hz and similar radial frequencies of $\omega_{y,z} = 2\pi \times 2180$ Hz ($\lambda = 13.5$). Using the same dimple wire with different experimental parameters, we have also been able to load the atoms into a third trap with even higher axial frequency of $\omega_x = 2\pi \times 320$ Hz and radial frequencies of $\omega_{y,z} = 2\pi \times 1520$ Hz ($\lambda = 4.75$) realizing an almost isotropic trap. We use forced radio-frequency (RF) evaporation to cool the gas close to or below the Bose-Einstein condensation threshold. As a direct consequence, colder gases contain less atoms, which in turn means that their corresponding critical temperature $T_c^* = \alpha^{1/3} T_c$ decreases as well. Here $T_c = \hbar \bar{\omega} k_B^{-1} (N/\zeta(3))^{1/3}$ where N is the total number of atoms, $\bar{\omega} = (\omega_x \omega_y \omega_z)^{1/3}$, \hbar and k_B are Planck and Boltzmann constants respectively and $\zeta(x)$ is the Riemann zeta function. To ensure thermal equilibrium of the gas we keep a constant RF knife for 200 ms at the end of the evaporative cooling ramp.

Comparison with ideal Bose gas theory

The constant α introduced in the main text is set in order that cooling the gas to $T_c^* = \alpha^{1/3} T_c$ coincides with the experimental observation of the appearance of a degenerate fraction of atoms ($N_{\text{bec}} \geq 0$). The value of α is slightly smaller than unity for the moderate trap aspect ratios ($\lambda = 4.75, 13.5$), which qualitatively agrees with theoretical studies of the shift of the critical temperature of interacting Bose gases [27]. For the most elongated trap ($\lambda = 113$), α is of the order of 7, which qualitatively agree with predictions of the degeneracy temperature for 1D systems [28].

Fit of the axial profile of the thermal fraction

Using an analytic expression for the density flux I of a freely expanding ideal Bose gas [12] and assuming an elliptical Gaussian shape for the excitation beams, hence neglecting any saturation effect, we deduce a formula describing the axial profile of density "slices" of the thermal fraction of expanding Bose gases

$$\rho_{\text{is}}(x) = \frac{1}{2\pi w} \int_{-\Delta t}^{\Delta t} dt \int dy dz \exp\left[-\frac{z^2}{2w^2}\right] I(x, y, z-z_0; t_0+t)$$

that we can use to fit our experimental results. Here t_0 is the expansion time, z_0 the position of the centre of the excitation laser beam profiles, $2\Delta t$ the exposure time and w the RMS width of the excitation beams. For the data presented in this work $t_0 = 46$ ms, $2\Delta t = 500$ μs and $w = 10$ μm [22]. This model depends on two parameters, the temperature of the gas T and its fugacity, which fixes the total number of atoms in

the thermal fraction of the gas N_{th} . To avoid the divergence of the population of the ground state of the system when the fugacity reaches its maximum, only the excited states of the ideal Bose gas are considered for the calculation of $\rho_{\text{is}}(x)$.

Estimation of the total atom number

Below the BEC threshold, in order to estimate the total number of atoms in the gas, we need to infer the total number of atoms in the condensed fraction of the system N_{bec} from the number of condensed atoms counted in a density slice measured with the fluorescence detector.

For traps with moderate aspect ratios ($\lambda = 4.75, 13.5$) we assume the condensed part of the system to behave as a pure BEC in the Thomas Fermi regime, which supposes $\mu \gg \hbar \omega_{x,y,z}$, where μ is the chemical potential of the BEC. This assumption is fulfilled quickly after passing the BEC threshold in these geometries. It is then possible to show that the expansion of the BEC along its different eigen-directions is well described by scaling laws whose parameters can be calculated numerically [29, 30]. We find scaling factors of 6 (axial) and 625 (radial) for $\lambda = 13.5$ and 28 (axial) and 430 (radial) for $\lambda = 4.75$ respectively. Including the detection process in the calculation is straightforward and we finally obtain a numerical formula which allows to deduce N_{bec} from the number of condensed atoms in a given density slice.

For the most anisotropic trap ($\lambda = 113$), we use an isotropic Gaussian ansatz for the radial density distribution of the degenerate fraction of the gas. Fitting the RMS width of the Gaussian along the y axis, it is then straightforward to infer N_{bec} from the number of atoms in the degenerate part of the cloud detected in a given density slice.

Normalisation of the fluctuations

When averaging the fluorescence pictures in order to obtain the density correlation function \mathbf{n}_2 , we average clouds with slightly different total atom numbers. These fluctuations can be corrected by normalizing \mathbf{n}_2 by the factor $1 + \text{Var}(S)/\bar{S}^2$, where S is the total fluorescence signal in each picture, \bar{S} its mean value for the considered clouds and $\text{Var}(S)$ its variance. This factor differs from one by less than a percent for all the data presented here. No further normalization is necessary in order to obtain \mathbf{n}_2 equal to unity at large distances Δx , Δy .

Density correlation function

The density correlation function is the sum of the two contributions \mathbf{g}_2 and \mathfrak{s} . The first term \mathbf{g}_2 can be expressed as $\mathbf{g}_2 = \bar{g}_2 * o^2$, where $\bar{g}_2(\Delta\mathbf{r})$ is an average of the second order correlation function $g_2(\mathbf{r}, \mathbf{r}')$ over the spatially inhomogeneous density profile of the gas with $\Delta\mathbf{r} = \mathbf{r} - \mathbf{r}'$ kept fixed, o^2 is the effective two-particle point spread function (PSF) of the fluorescence imaging and $*$ is the convolution product. The function o^2 accounts for the diffusion of single atoms during the imaging process and optics aberrations, which blur the position of single atoms in the images [22]. The other contribution to the density correlation function \mathfrak{s} is due to the

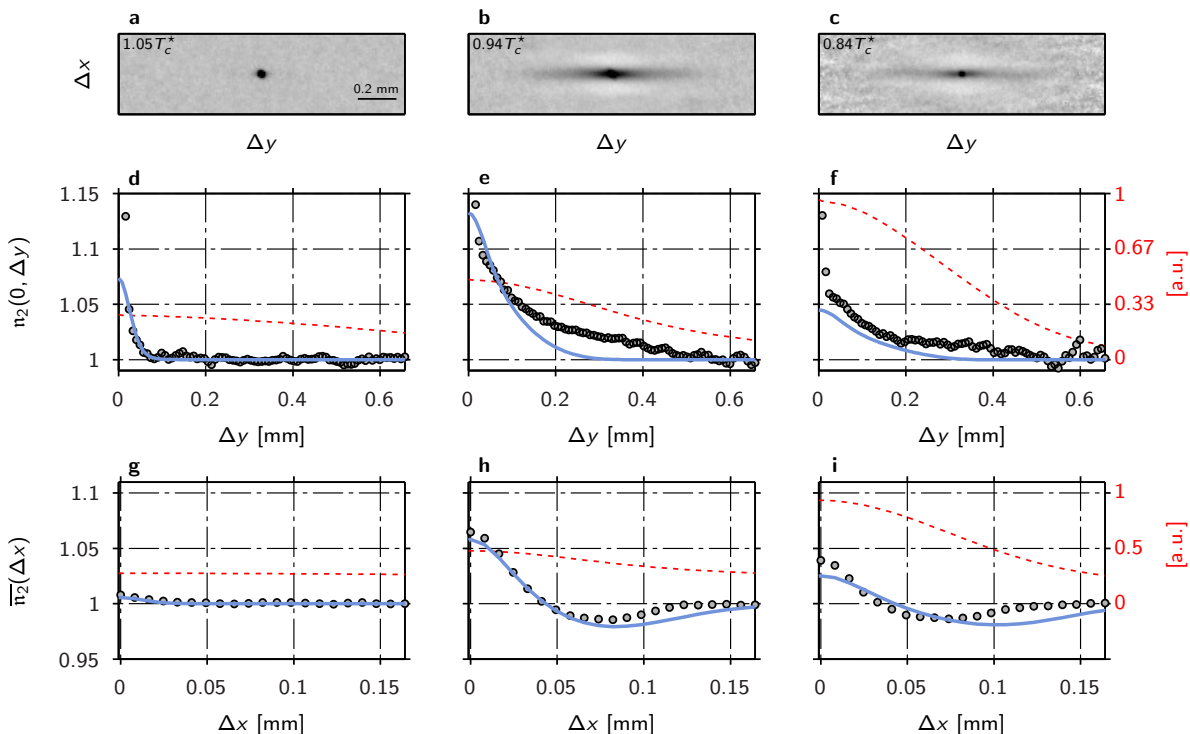


FIG. 4. **a,b,c**, Density correlation function of expanding Bose gases n_2 (lateral cut in $(\Delta x, \Delta y)$ plane) at $1.05 T_c^*$, $0.94 T_c^*$, and $0.84 T_c^*$, the aspect ratio of the atomic source λ is 4.75. **d,e,f**, (circles) Radial cuts of **a,b** and **c**. (dashed line) Radial cuts of the corresponding autocorrelation of the mean density profile. (solid line) Radial cuts of ideal Bose gas theory's predictions for the second order correlation function $g_2(0, \Delta y)$. **g,h,f**, (circles) Radially averaged axial cuts of **a,b** and **c** over $160 \mu\text{m}$ where the shot noise peak \mathfrak{s} is spatially excluded. The width of the exclusion region is $32 \mu\text{m}$. (dashed line) Radially averaged axial cuts of the corresponding autocorrelation of the mean density profile. (solid line) Radially averaged axial cuts of ideal Bose gas theory's predictions for the second order correlation function $\bar{g}_2(\Delta x)$.

atomic shot noise and is proportional to the inverse of the mean density of the gas.

In [12], an analytical expression for the second order correlation function of an ideal Bose gas after free expansion is presented. Here we slightly extend the model in order to take into account the imaging scheme. Using a 2D isotropic Gaussian model for the two-particle PSF o^2 allows to derive an analytic expression for g_2 which can be calculated numerically.

Imaging resolution

The resolution of the fluorescence imaging is to a large extent determined by the diffusion of atoms during the detection process [22]. Hence, each individual atom appears as a *fluorescence pattern*, composed of typically 5 detected photons randomly distributed over a few adjacent pixels. The broadening of the atomic shot noise peak \mathfrak{s} is given by the mean

autocorrelation of the fluorescence patterns. Its elliptic shape reflects the increased diffusion of the atoms along the direction of the excitation beams. It is modelled by a 2D Gaussian with eigen-axes rotated by 45° and fitted RMS widths $\sqrt{2} \times 5.5 \mu\text{m}$ and $\sqrt{2} \times 6.2 \mu\text{m}$. However, \mathfrak{s} is insensitive to the random offset of each fluorescence pattern centroid with respect to the actual position of the corresponding atom. This offset has to be included in a full description of the imaging resolution, yielding the two-particle PSF o^2 .

Assuming a 2D isotropic Gaussian model for o^2 , we can estimate its RMS width from the observed axial width of g_2 above the condensation threshold. The RMS width of \bar{g}_2 , related to the axial coherence length of the gas [6], is expected to be much smaller than the observed RMS width of g_2 . Thus, we assume the latter to originate only from the finite resolution (see Fig. 2g). This explains the reduction of $g_2(0)$ below 2 for systems close or above the BEC threshold [6]. As the observed width stems from a two-particle correlation, it is sensitive to the actual resolution of the system, including the centroid offset. Finally, we obtain a value of $\sqrt{2} \times 8 \mu\text{m}$ for the RMS width of o^2 .

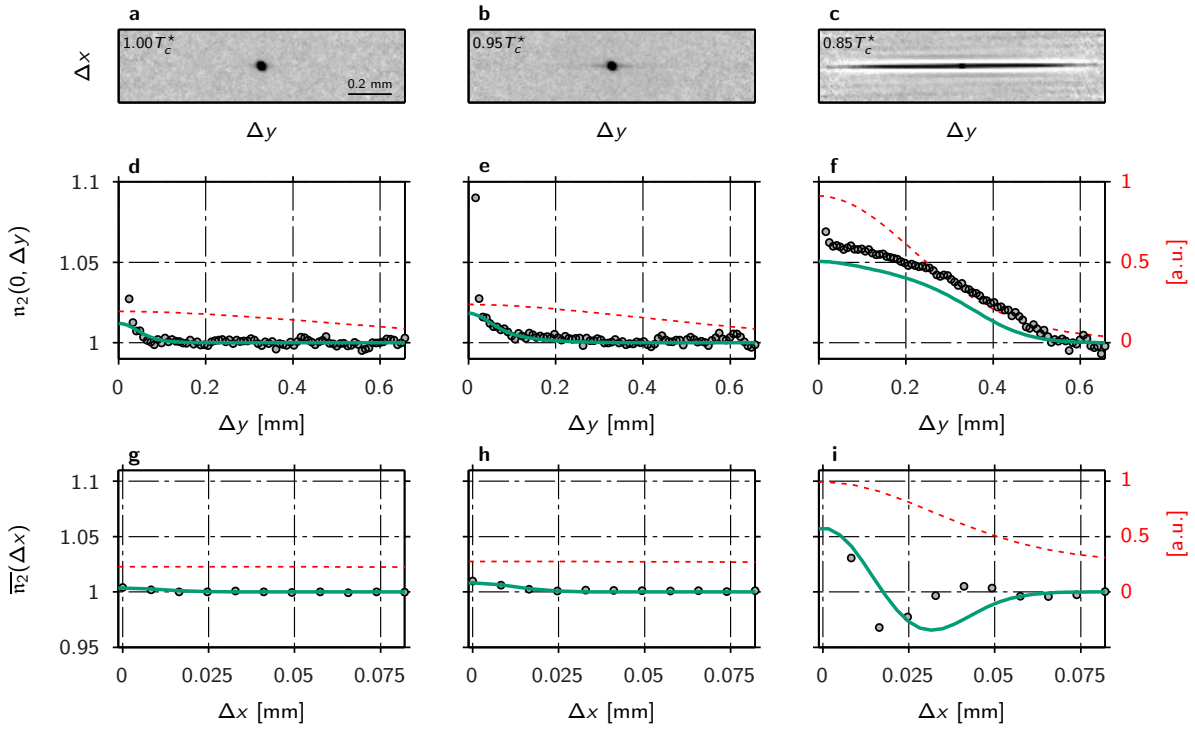


FIG. 5. **a,b,c**, Density correlation function of expanding Bose gases n_2 (lateral cut in $(\Delta x, \Delta y)$ plane) at $1.00T_c^*$, $0.95T_c^*$, and $0.85T_c^*$, the aspect ratio of the atomic source λ is 113. **d,e,f**, (circles) Radial cuts of **a,b** and **c**. (dashed line) Radial cuts of the corresponding autocorrelation of the mean density profile. (solid line) Radial cuts of ideal Bose gas theory's predictions for the second order correlation function $g_2(0, \Delta y)$. **g,h,f**, (circles) Radially averaged axial cuts of **a,b** and **c** over $160 \mu\text{m}$ where the shot noise peak \mathfrak{s} is spatially excluded. The width of the exclusion region is $32 \mu\text{m}$. (dashed line) Radially averaged axial cuts of the corresponding autocorrelation of the mean density profile. (solid line) Radially averaged axial cuts of ideal Bose gas theory's predictions for the second order correlation function $\bar{g}_2(\Delta x)$.